ACS APPLIED MATERIALS & INTERFACES

Research Article

www.acsami.org

Three-Dimensional Graphene Oxide Nanostructure for Fast and Efficient Water-Soluble Dye Removal

Fei Liu, Soyi Chung, Gahee Oh, and Tae Seok Seo*

Department of Chemical and Biomolecular Engineering (BK21 program) and Institute for the BioCentury, Korea Advanced Institute of Science and Technology (KAIST), 291 Daehak-ro, Yuseong-gu, Daejeon, 305-701, Republic of Korea.

Supporting Information

ABSTRACT: In this study, we demonstrated the potential of graphene nanomaterials as environmental pollutant adsorbents by utilizing the characteristics of ultralarge surface area and strong $\pi-\pi$ interaction on the surface. We generated a three-dimensional (3D) graphene oxide sponge (GO sponge) from a GO suspension through a simple centrifugal vacuum evaporation method, and used them to remove both the methylene blue (MB) and methyl violet (MV) dyes which are main contaminants from the dye manufacturing and textile finishing. The efficiency and speed of dye adsorption on a GO sponge was investigated under various parameters such as contact time, stirring speed, temperature, and pH. The adsorption process shows that 99.1% of MB and 98.8% of MV have been removed and the equilibrium status has been reached in 2 min. The 3D GO sponge displays adsorption capacity as high as 397 and 467 mg g^{-1} for MB and MV dye, respectively, and the kinetic data reveal that the adsorption process of MB and MV dyes is well-matched with the pseudo second-order model. The MB and MV adsorption on the 3D GO sponge involved in endothermic chemical adsorption through the strong $\pi-\pi$ stacking and anion−cation interaction with the activation energy of 50.3 and 70.9 kJ mol^{-1}, respectively. The 3D GO sponge has demonstrated its high capability as an organic dye scavenger with high speed and efficiency.

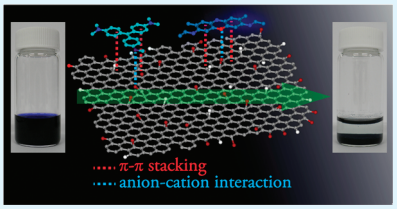

KEYWORDS: *3D graphene oxide, graphene, methyl violet, methylene blue, adsorption*

INTRODUCTION

Improvement of the decontamination efficiency for certain organic pollutants through eco-friendly adsorption techniques has become an important issue in the fields of environmentology.[1,2] In particular, dyes and pigments, which are the main organic pollutant compound from the dye manufacturing and textile branches, have been an issue to be removed from contaminated water.[3] A number of sorbent materials including mesoporous silica,[4] mesoporous hybrid xerogel,[5] caly,[6] activated carbon,[7] sepiolite,[8,9] and pansil[9] have been studied for eliminating water-soluble organic dyes like procion red MX-5B, methylene blue (MB), methyl violet (MV), and rhodamine-B. Among them, carbon-based nanomaterials of graphite,[10] fullerene[11,12] and carbon nanotube (CNT),[13−18] which play a major role in the fields of electronics and sensors, demonstrated their capability as an effective sorbent for inorganic and organic contaminants. For instance, single- and multiwalled CNTs have shown stronger binding affinity with heavy metal ions of Zn,[19] Ni,[20] Pd,[21] Co,[22] and organic pollutants of phenolic compounds,[23] naphthalene,[24] and chlorobenzene[25] through the combination of hydrophobic, electrostatic, and $\pi-\pi$ stacking interaction. However, these engineered carbon materials require high-cost fabrication process such as chemical vapor deposition, and suffer from low water dispersibility and metal catalytic impurities. Therefore, the development of a novel synthetic method for carbon-based sorbent materials and the improvement of the adsorption efficiency are still demanded.

Graphene, which is a basic unit for construction of carbonaceous materials and is composed of two-dimensional sp^2 carbon network with a honeycomb crystal structure, has demonstrated its unusual properties such as high electron mobility, high opacity due to an atomic monolayer, high thermal conductivity, and extraordinary mechanical strength, making it a next-generation nanomaterial to be applied for nanoelectronics, nanocomposites, nanosensors, and nano-devices.[26−31] An additional unique feature of graphene compared with other carbon allotropes is an ultralarge specific surface area (2,630 m^2 g^{-1}) and flat structure,[32−36] which provide ideal characteristics as an excellent adsorbent. Recent studies have presented that individual graphene oxide sheets can be produced in a large scale by exfoliating from the cheap graphite, and their surface can be modified with organic and biomolecules through strong $\pi-\pi$ stacking interaction and van der Waals forces.[36−39] Moreover, the suspended graphene oxide solution can be reassembled to form a various dimensional structure and can be utilized as a supporting platform for adsorbing a large quantity of inorganic, organic and biomolecules. In this regard, GO and GO/iron oxide nanoparticle composites have been used for removing organic dyes.[40−44] Single-layered GO solution demonstrated high adsorption capacity due to the homogeneity and large surface area of GO. However, in the recovery process for dye adsorbed

Received: November 15, 2011
Accepted: December 29, 2011
Published: December 29, 2011

GO, ultrahigh centrifugation for a prolonged time is necessary to collect the highly dispersed GO.[40−42] Otherwise, unprecipitated nanosized GO may lead to another nanotoxic material in the environments. In case of GO/iron oxide nanoparticle composites, the recovery step was conducted with ease by using the external magnetic field, but the presence of the iron oxide nanoparticles on the surface caused the reduced adsorption area and surface charge on GO, resulting in long adsorption time and 6-fold less adsorption capacity than the GO.[43,44]

Herein, we have demonstrated that the use of three-dimensional (3D) graphene materials as environmental pollutant scavengers by utilizing the microporous structure with ultralarge surface area and strong $\pi-\pi$ interaction on the surface. We generated a 3D GO sponge from a GO suspension through a simple centrifugal vacuum evaporation method, and explored the potential of GO sponges to remove both the MV and MB dyes, and their facile recovery after dye adsorption on the GO sponges. Kinetic study, adsorption mechanism, and thermodynamic analysis on the dye adsorption were investigated.

EXPERIMENTAL PROCEDURES

Chemicals and Measurements. Methylene blue (MB) [$C_{16}H_{18}N_3OS$, MW: 333.6 g mol^{-1}, λ_{max}: 630 nm], methyl violet (MV) [$C_{25}H_{30}N_3Cl$, MW: 393.96 g mol^{-1}, λ_{max}: 584 nm], and graphite flakes were purchased from Sigma-Aldrich. All MB and MV aqueous solutions used in this study were prepared by dissolving a certain amounts of MB and MV in deionized water. The morphologies of 3D graphene oxide sponge before and after adsorption with dyes have been characterized by scanning electron microscopy (SEM) (Nova230 FEI). The composition of GO sheets was investigated by X-ray photoelectron spectroscopy (Thermo VG Scientific). The specific surface area of 3D GO sponge was estimated by using a Brunauer−Emmett−Teller (BET) method. The height and morphology of GO sheets were recorded by atomic force microscope (AFM, Veeco D3100, USA) in tapping mode and a 512 × 512 pixel resolution.

Fabrication of a 3D GO Sponge. An illustration for generating a GO sponge in a speed vacuum concentrator is presented in Figure 1a. The homogeneous suspension of single-layered GO sheets was produced by sonication of graphite oxide in an aqueous solution according to the modified Hummers method (see Figure S1 and S2 in the Supporting Information).[45] Graphene oxide sponge was fabricated by employing a centrifugal vacuum system.[46] In brief, 1 mL of GO colloidal suspension (10 mg mL^{-1}) was prepared in a 2 mL Eppendorf tube, and then the tube was placed on the rotor plate fixed in the vacuum chamber. Graphene oxide sponge was generated when the centrifugal vacuum evaporator was operated at a rotating speed of 1800 rpm with a pressure of 1 × 10^{-4} Torr at room temperature for 6 h.

Dye Adsorption on a 3D GO Sponge. Dye adsorption experiments on a 3D GO sponge have been performed by mixing 5 mL of a dye solution (1.2× 10^{-3} or 2.4 × 10^{-3} M of concentration) with 10 mg GO sponge. The temperature of the mixture solution was controlled in a water bath at 298, 323, and 343 K, and a stirring rate was adjusted at 100, 200, and 300 rpm. The pH was fixed at 3, 7, and 10 by using HCl or NaOH, and the pH value was determined by using an Orion* 4-Star Plus pH/ISE Benchtop Multiparameter Meter (Thermal Electron Corporation). A 20 μL of sample was continuously taken and diluted with 580 μL DI water for adsorption analysis at appropriate time intervals (0, 2, 4, 6, 8, 10, 15, 20, 30, 40, 50, 60, 90, 120, 150, 180 min), and the adsorbed amount of dyes was calculated by Beer's law based on the absorption peak at 630 nm for MB and 584 nm for MV by using UV−vis spectrophotometer (UV-2450, SHIMADZU). After adsorption, the dye adsorbed GO sponge was filtered on a cellulose acetate membrane which has a pore size of 200 nm (ADVANTEC), and the total carbon (TC) content of filtrate was determined by a CS-800 Carbon/Sulfur determinator (CS800, ELTRA).

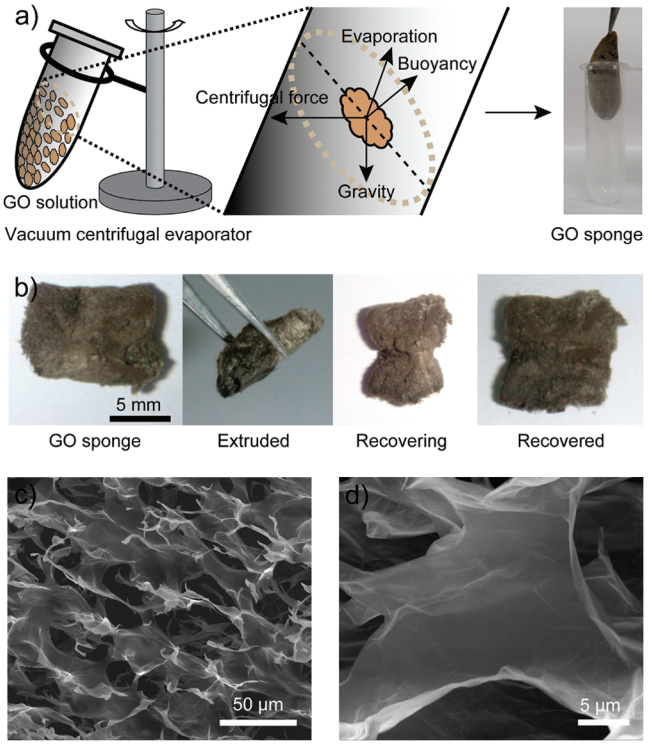

Figure 1. (a) Synthetic scheme of a 3D GO sponge. (b) Flexibility test of a GO sponge. (c) Low-magnification of SEM image for the GO sponge surface and (d) high-magnification of SEM image for the inner part of the 3D GO sponge.

RESULTS AND DISCUSSION

Synthesis and Characteristics of a 3D GO Sponge. The synthetic scheme of the 3D GO sponge is illustrated in Figure 1a. One milliliter of an aqueous GO solution (10 mg mL^{-1} concentration) prepared in a 2 mL Eppendorf tube has been transformed into a 3D GO sponge via a vacuum evaporation process. The GO sheets in a colloidal suspension were simply assembled by the combination of the vertical evaporation and outward centrifugal force. If the vacuum evaporation process is operated at low temperature, the centrifugal force is dominant over the evaporation force, generating a GO assembled lump on the tube wall. The resultant GO sponge which displayed a brown color and cottonlike soft morphology was easily obtained from the Eppendorf tube by using tweezers. Figure 1b demonstrated the flexibility of the GO sponge by showing that the extruded 3D GO structure was recovered into its own original shape in a short time.

The SEM image of the GO sponge at a low magnification resolution shows that the GO sheets were well-assembled and interconnected with relatively homogeneous pore size of tens of micrometers, and reveals that the single layered GO sheets, originally ranging from 200 nm to 5 μm in the lateral dimension, were self-assembled to form 30 μm size flakes which were cross-linked by mainly edge-to-edge and partially edge-to-surface to build a 3D network with 48.4097 m^2/g of BET surface area (Figure 1c). The inner part of the GO sponge also had a uniform porous structure with parallel GO sheet connection due to the ordered stacking derived from the centrifugal force during vacuum evaporation (see Figure S3 in

the Supporting Information). The representative GO flake in Figure 1d shows a very smooth and large surface with a size of more than 20 μm. Such organized and 3D interconnected graphene sheets contribute to high mechanical strength and structural stability of GO sponge and the exposed graphene surface can serve as an advanced adsorbent platform to remove the environmentally pollutant organic dyes. Based upon this hypothesis, we investigated the adsorption efficiency and mechanism of MB and MV dye on a GO sponge with variation of stirring speed, temperature and pH.

Kinetic Analysis of MB and MV Adsorption on the GO Sponge. The chemical structure of MB and MV has rich aromatic rings and cationic atoms (S^+ in MB and N^+ in MV) (Figure 2a) which are favorable for adsorbing on the GO

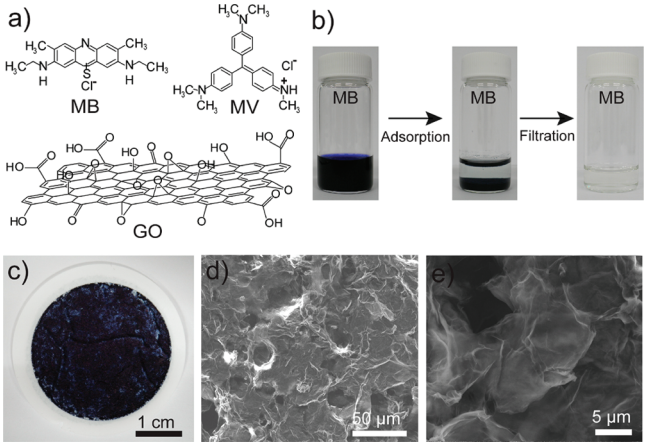

Figure 2. (a) Chemical structures of MB, MV, and GO. (b) Digital images of the original MB dye solution (left), the pale color solution with precipitated MB adsorbed GO sponges (middle), and the colorless water after filtering the MB adsorbed GO sponge (right). (c) Digital image of the filtered dye adsorbed GO sponges. SEM images of the MB adsorbed GO sponges with (d) low-magnification and (e) high-magnification.

surface through $\pi-\pi$ stacking and ionic interaction. For instance, an MB dye solution (conc. of 1.2×10^{-3} M) which initially displays very dark-blue color was changed into a very pale color solution upon addition of 10 mg GO sponge in only 2 min at room temperature, and the vacuum filtration results in clean and colorless water as shown in Figure 2b. Due to the hydrophilic property of GO and 3D condensed framework, the GO sponge are well dispersed in an aqueous phase and remove the MB efficiently during mixing. The precipitated dye adsorbed GO sponge was filtered and the TC of the filtrate was measured as 0.0461 wt %, while that of the original MB solution was 0.3671 wt %. The morphology of the recovered GO sponge was changed from lumps into millimeter-sized GO particulates which were easily and quickly collected through a simple vacuum filtration (Figure 2c). If the homogeneous 2D GO sheets were employed as an adsorbent, it is somewhat difficult to collect the nanosized GO completely, which could cause secondary environmental pollution and the ultrahigh centrifugation is time-consuming. Therefore, the 3D GO sponge has an advantage over the 2D GO sheets in terms of recovery process for dye adsorbed GO. The SEM image of the dye adsorbed GO particulates shows the collapsed pore structure, the thicker and rough GO layer, and the aggregated shape which may be derived from the water solubility of GO as well as the enhanced $\pi-\pi$ stacking of GO owing to the adsorbed dye molecules (Figure 2d, e). These results demonstrate that the hydrophilic GO sponge were mixed rapidly in an aqueous dye solution and played a role as an excellent adsorbent to capture aromatic organic dyes via significant $\pi-\pi$ interaction and anion−cation interaction.

We evaluated the adsorption rate of MB and MV by plotting between adsorbed amounts (q_t: mg g^{-1}) and different stirring speeds from 100 to 300 rpm at room temperature with a concentration of 1.2×10^{-3} M. The adsorption rate was quite fast for both MB (99.5 mg g^{-1} min^{-1}) and MV (116.5 mg g^{-1} min^{-1}), and a majority of the dyes were removed within 2 min (see Figure S4 in the Supporting Information). The removal efficiency was calculated as 99.9% for both MB and MV dyes. In case of MB, it has similar tendency at 200 and 300 rpm, but adsorption rate at 100 rpm became slower. For MV, the adsorption rate is almost equivalent regardless of the stirring rate. So we repeated those experiments by doubling the concentration of MB and MV (2.4×10^{-3} M) to demonstrate the high adsorption efficiency of GO sponge. Figure 3a and 3b

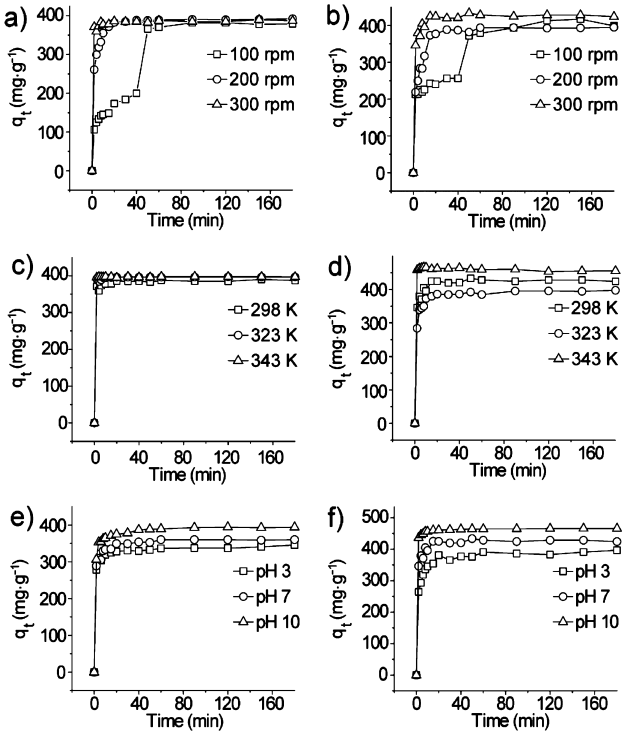

Figure 3. Effect of stirring rate on the adsorption rate of (a) MB and (b) MV dyes. The effect of temperature on the adsorption rate of (c) MB and (d) MV dyes. The effect of pH on the adsorption rate of (e) MB and (f) MV dyes.

show the MB and MV adsorption kinetic profiles at different stirring rate from 100 to 300 rpm at room temperature. The higher stirring speed produced the faster adsorption rate although the difference of adsorption rate between 200 and 300 rpm was minimal. At 100 rpm, both MB and MV reached a saturated level around 60 min, while 20 min was required for 300 rpm, implying that the mixing speed is one of the important factors for rapid dye removal. Therefore, we fixed 300 rpm of stirring rate for further experiments. A study on the effect of temperature for the adsorption rate was conducted at 298, 323, and 343 K under the conditions of 2.4×10^{-3} M dye

dx.doi.org/10.1021/am201590z | ACS Appl. Mater. Interfaces 2012, 4, 922−927

concentration, 300 rpm and pH 7. When the reaction temperature was increased from 298 to 343 K, the equilibrium status has been reached in 2 min. The amount of dye loaded on the GO sponge increased from 387 to 397 mg g^{-1} for MB and from 384 to 467 mg g^{-1} for MV (Figure 3c, d), indicating that the adsorption process was endothermic, and the adsorption efficiency was 99.1% for MB and 98.8% for MV. The thermal energy allows the dye adsorbate to diffuse across the external boundary layer of graphene and into the internal pores of the GO sponge to enhance the quantity of adsorbed dye molecules, resulting in the higher saturated equilibrium level. The effect of pH on the adsorption rate of MB and MV on the GO sponge was examined at pH ranging from 3 to 10 with 2.4×10^{-3} M concentration, 300 rpm and 298 K. Since the GO surface becomes abundant with negatively charged functional groups at high pH value, the ionic interaction in addition to $\pi-\pi$ stacking would be reinforced to bind the cationic dye molecules on the surface. Figure 3e and 3f show that the amount of the adsorbed MB and MV on the GO sponge increased in proportion to pH value due to the enhanced degree of ionization of GO sponge and the ionic interaction with cationic MB and MV. These results represent that the loaded quantity was 328 mg g^{-1} at pH 3 and 374 mg g^{-1} at pH 10 for MB, whereas those values were 380 mg g^{-1} at pH 3 and 460 mg g^{-1} at pH 10 for MV, demonstrating that the adsorption capability was improved by 14% for MB and 21% for MV at pH 10 in comparison with pH 3. Both of the adsorption kinetics, however, was very fast (153 mg g^{-1} min^{-1} for MB and 218 mg g^{-1} min^{-1} for MV) regardless of pH value, and the equilibrium plateau was reached within 20 min.

Mechanism and Thermodynamic Analysis of MB and MV Adsorption on the GO Sponge. The adsorption mechanism of MB and MV on the 3D GO sponge has been examined by using pseudo first-order, pseudo second-order and intraparticle diffusion models.[8,9] Dye adsorption experiments were performed at 298, 323, and 343 K under the conditions of pH 7 and at 300 rpm of stirring rate, and then the experimental data were fitted into the above-mentioned models. When the pseudo first-order model is applied, the correlation coefficient values for adsorption of MB and MV varied from 0.03071 to 0.59684 and from 0.08247 to 0.66257 respectively, meaning the pseudo first-order kinetic model was not matched (see Table S1 in the Supporting Information). However, the pseudo second-order kinetic equation produced the correlation coefficients close to 1 within 0.03% variation as shown in Figure 4a,b and Table 1, which means that the dye adsorption on a sponge agrees with the pseudo second-order model.

Adsorption mechanisms can be described by successive process of dye diffusion through the boundary layer, intraparticle diffusion, and dye adsorption on the GO surface. According to Weber-Morris theory which assumes intraparticle diffusion as a rate-controlling factor,[9] the plot between the adsorption capacity (q_t) and the square root of time ($t^{0.5}$) should generate a straight line. Table 2 shows the values of intraparticle diffusion parameters for MB and MV adsorption at 298, 323, and 343 K on the GO sponge. Figure 4c,d shows at least two steps involved during the adsorption process at 298 and 323 K because the two sections with different linear slope appeared.[8,9] Judged from Figures 2 and 3, those two slopes can be explained by two distinct diffusion phenomena: First, dye molecules are penetrating through the macropores of GO sponges and saturated on the external surface until 20 min, and then the pores are diminished resulting in the decreased

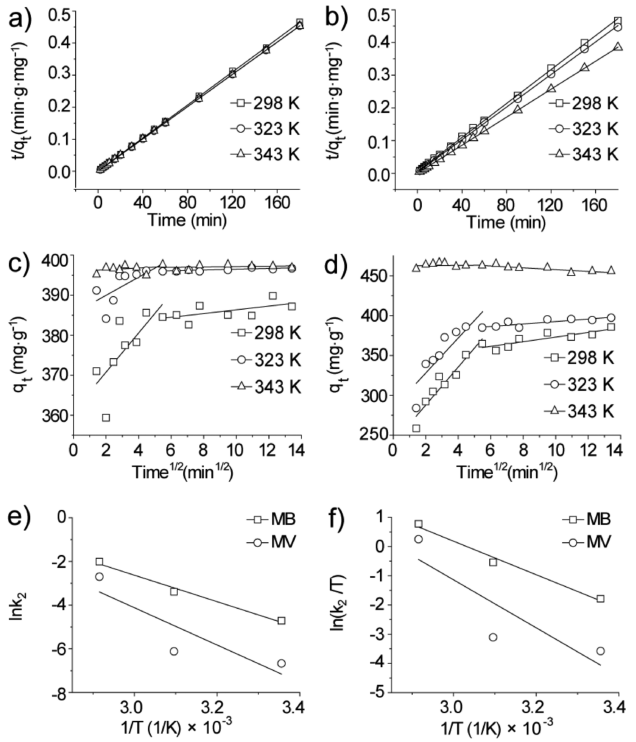

Figure 4. Plot of a pseudo second-order model for (a) MB and (b) MV adsorption, and intraparticle diffusion model for (c) MB and (d) MV adsorption. (e) Arrhenius plot and (f) Eyring plot for MB and MV adsorption on the GO sponge.

Table 1. Coefficients of a Pseudo Second-Order Diffusion Model for MB and MV Adsorption on the GO Sponge

T (K)	$q_{e,exp}$ (mg g^{-1})	$q_{e,cal}$ (mg g^{-1})	k_2(g mg^{-1} min^{-1})	R^2
Pseudo Second-Order Model of MB				
298	389.84	387.59689	0.008968448	0.99995
323	396.89	396.82539	0.033767767	1
343	397.65	396.82539	0.133356013	1
Pseudo Second-Order Model of MV				
298	385.6637365	384.6153846	0.001268293	0.9996
323	402.6763275	401.6064257	0.002198617	0.9998
343	467.2161569	467.2897196	0.067140798	1

Table 2. Coefficients of an Intraparticle Diffusion Model for MB and MV Adsorption on the GO Sponge

T (K)	k_{i1}(mg g^{-1} $min^{-0.5}$)	k_{i2}(mg g^{-1} $min^{-0.5}$)	R_1^2	R_2^2
Intraparticle Diffusion Model of MB				
298	4.86139	0.47077	0.48122	0.27586
323	2.26852	0.10621	0.41997	0.6553
343	0.21733	0.04865	−0.06272	−0.11421
Intraparticle Diffusion Model of MV				
298	23.74223	2.91174	0.90217	0.90217
323	22.17461	5.88158	0.71352	0.67422
343	4.48949	0.56019	0.83916	0.82832

diffusion rate of dye. However, the single slope of 343 K implies that diffusion rate was not influenced significantly during the entire adsorption process probably due to the enough thermal energy to overcome the barrier passing through the reduced cavity of GO sponge. Second, the activation energy and Arrhenius factor of MB and MV adsorption were estimated according to the Arrhenius equation. As shown in Figure 4e,

dx.doi.org/10.1021/am201590z | ACS Appl. Mater. Interfaces 2012, 4, 922−927

the activation energy of MB and MV are 50.3 and 70.9 kJ mol^{-1}, respectively. Physical adsorption process is known to have activation energy of 5−40 kJ mol^{-1}, whereas chemical adsorption has a higher activation energy of 40−800 kJ mol^{-1}. Therefore, MB and MV adsorption on the 3D GO sponge is assumed to be chemical adsorption through the strong $\pi-\pi$ stacking and anion−cation interaction. Enthalpy of activation was derived from Eyring equation, revealing those values of MB and MV are 47.7 and 68.2 kJ mol^{-1}, respectively (Figure 4f).

CONCLUSIONS

We have demonstrated a facile fabrication method for 3D GO sponges by a simple centrifugal vacuum evaporation, and its high potential for organic pollutant dye removal. The adsorption process was complete with high efficiency of 99.1% for MB and 98.8% for MV in 2 min, and the dye adsorbed GO sponges were quickly recovered by simple vacuum filtration. The adsorption kinetics of MB and MV on the GO sponge was investigated as a function of stirring rate, temperature, and pH. The adsorption kinetics was followed by the pseudo second-order model with an endothermic reaction. These results prove that the applicability of graphene nanomaterials can be expanded to not only nanoelectronics but also in the fields of environmentology.

ASSOCIATED CONTENT

Supporting Information

(1) Low-magnification of SEM image for the inner part of the 3D GO sponge (Figure S1), (2) the effect of stirring speed on the adsorption rate of MB and MV with concentration of 1.2×10^{-3} M (Figure S2), and (3) the coefficients of pseudo first-order diffusion model for MB and MV adsorption on the GO sponge (Table S1). This material is available free of charge via the Internet at http://pubs.acs.org/.

AUTHOR INFORMATION

Corresponding Author

*Tel: +82- 42-350-3933. Fax: +82- 42-350-3910. E-mail: seots@kaist.ac.kr.

ACKNOWLEDGMENTS

This work was supported by the Converging Research Center Program funded by the Ministry of Education, Science and Technology (2011K000837).

REFERENCES

(1) Meunier, B. *Science* **2002**, *296*, 270−271.
(2) Ma, W.; Li, J.; Tao, X.; He, J.; Xu, Y.; Yu, J. C.; Zhao, J. *Angew. Chem., Int. Ed.* **2003**, *42*, 1029−1032.
(3) Janoš, P. *Environ. Sci. Technol.* **2003**, *37*, 5792−5798.
(4) Ho, K. Y.; Mckay, G.; Yeung, K. L. *Langmuir* **2003**, *19*, 3019−3024.
(5) Wu, Z.; Joo, H.; Lee, K. *Chem. Eng. J.* **2005**, *112*, 227−236.
(6) Haderlein, S. B.; Weissmahr, K. W.; Schwarzenbach, R. P. *Environ. Sci. Technol.* **1996**, *30*, 612−622.
(7) Mohammadi, M.; Hassani, A. J.; Mohamed, A. R.; Najafpour, G. D. *J. Chem. Eng. Data* **2010**, *55*, 5777−5785.
(8) Doğan, M.; Özdemir, Y.; Alkan, M. *Dyes Pigm.* **2007**, *75*, 701−713.
(9) Weber, W. J.; Morris, J. C. *J. Sanit. Eng. Div. ASCE* **1963**, *89*, 31−59.
(10) Jaegfeldt, H.; Kuwana, T.; Johansson, G. *J. Am. Chem. Soc.* **1983**, *105*, 1805−1814.
(11) Cheng, X.; Kan, A. T.; Tomson, M. B. *J. Chem. Eng. Data* **2004**, *49*, 675−683.
(12) Mchedlov-Petrossyan, N. O.; Klochkov, V. K.; Andrievsky, G. V.; Ishchenko, A. A. *Chem. Phys. Lett.* **2001**, *341*, 237−244.
(13) Long, R. Q.; Yang, R. T. *J. Am. Chem. Soc.* **2001**, *123*, 2058−2059.
(14) Basiuk (Golovataya-Dzhymbeeva), E. V.; Rybak-Akimova, E. V.; Basiuk, V. A.; Acosta-Najarro, D.; Saniger, J. M. *Nano Lett.* **2002**, *2*, 1249−1252.
(15) Zhang, J.; Lee, J. -K.; Wu, Y.; Murray, R. W. *Nano Lett.* **2003**, *3*, 403−407.
(16) Yan, Y.; Zhang, M.; Gong, K.; Su, L.; Guo, Z.; Mao, L. *Chem. Mater.* **2005**, *17*, 3457−3463.
(17) Wu, C. *J. Hazardous Mater.* **2007**, *144*, 93−100.
(18) Yao, Y.; Xu, F.; Chen, M.; Xu, Z.; Zhu, Z. *Bioresour. Technol.* **2010**, *101*, 3040−3046.
(19) Cho, H. H.; Wepasnick, K.; Smith, B. A.; Bangash, F. K.; Fairbrother, D. H.; Ball, W. P. *Langmuir* **2010**, *26*, 967−981.
(20) Lu, C. Y.; Liu, C.; Rao, G. P. *J. Hazard. Mater.* **2008**, *151*, 239−246.
(21) Tian, X.; Zhou, S.; Zhang, Z.; He, X.; Yu, M.; Lin, D. *Environ. Sci. Technol.* **2010**, *44*, 8144−8149.
(22) Chen, S. Z.; Liu, C.; Yang, M.; Lu, D.; Zhu, L.; Wang, Z. *J. Hazard. Mater.* **2009**, *170*, 247−251.
(23) Lin, D.; Xing, B. *Environ. Sci. Technol.* **2008**, *42*, 7254−7259.
(24) Cho, H.; Smith, B. A.; Wnuk, J. D.; Fairbrother, D. H.; Ball, W. P. *Environ. Sci. Technol.* **2008**, *42*, 2899−2905.
(25) Chen, W.; Duan, L.; Zhu, D. *Environ. Sci. Technol.* **2007**, *41*, 8295−8300.
(26) Novoselov, K. S.; Geim, A. K.; Morozov, S. V.; Jiang, D.; Zhang, Y.; Dubonos, S. V.; Grigorieva, I. V.; Firsov, A. A. *Science* **2004**, *306*, 666−669.
(27) Jiang, H. *Small* **2011**, *7*, 2413−2427.
(28) Huang, X.; Qi, X.; Boey, F.; Zhang, H. *Chem. Soc. Rev.* **2012**, DOI: 10.1039/C1CS15078B.
(29) Huang, X.; Yin, Z.; Wu, S.; Qi, X.; He, Q.; Zhang, Q.; Yan, Q.; Boey, F.; Zhang, H. *Small* **2011**, *7*, 1876−1902.
(30) Song, Y.; Qu, K.; Zhao, C.; Ren, J.; Qu, X. *Adv. Mater.* **2010**, *22*, 2206−2210.
(31) Song, Y.; Wei, W.; Qu, X. *Adv. Mater.* **2011**, *23*, 4215−4236.
(32) Balapanuru, J.; Yang, J. X.; Xiao, S.; Bao, Q.; Jahan, M.; Polavarapu, L.; Wei, J.; Xu, Q. H.; Loh, K. P. *Angew. Chem., Int. Ed.* **2010**, *49*, 6549−6553.
(33) Tang, Z.; Shen, S.; Zhuang, J.; Wang, X. *Angew. Chem., Int. Ed.* **2010**, *49*, 4603−4607.
(34) Lee, S. H.; Kim, H. W.; Hwang, J. O.; Lee, W. J.; Kwon, J.; Bielawski, C. W.; Ruoff, R. S.; Kim, S. O. *Angew. Chem., Int. Ed.* **2010**, *49*, 10084−10088.
(35) Park, S.; Ruoff, R. S. *Nat. Nanotechnol.* **2009**, *4*, 217−224.
(36) Behabtu, N.; Lomeda, J. R.; Green, M. J.; Higginbotham, A. L.; Sinitskii, A.; Kosynkin, D. V.; Tsentalovich, D.; Parra-Vasquez, A. N. G.; Schmidt, J.; Kesselman, E.; Cohen, Y.; Talmon, Y.; Tour, J. M.; Pasquali, M. *Nat. Nanotechnol.* **2010**, *5*, 406−411.
(37) Stankovich, S.; Dikin, D. A.; Dommett, G. H. B.; Kohlhaas, K. M.; Zimney, E. J.; Stach, E. A.; Piner, R. D.; Nguyen, S. B. T.; Ruoff, R. S. *Nature* **2006**, *442*, 282−286.
(38) Qi, X.; Pu, K.; Li, H.; Zhou, X.; Wu, S.; Fan, Q.; Liu, B.; Boey, F.; Huang, W.; Zhang, H. *Angew. Chem., Int. Ed.* **2010**, *49*, 9426−9429.
(39) Qi, X.; Pu, K.; Zhou, X.; Li, H.; Liu, B.; Boey, F.; Huang, W.; Zhang, H. *Small* **2010**, *6*, 663−669.
(40) Ramesha, G. K.; Kumara, A. V.; Muralidhara, H. B.; Sampath, S. *J. Colloid Interface Sci.* **2011**, *361*, 270−277.
(41) Yang, S.; Chen, S.; Chang, Y.; Cao, A.; Liu, Y.; Wang, H. *J. Colloid Interface Sci.* **2011**, *359*, 24−29.
(42) Gao, W.; Majumder, M.; Alemany, L. B.; Narayanan, T. N.; Ibarra, M. A.; Pradhan, B. K.; Ajayan, P. M. *ACS Appl. Mater. Interfaces* **2011**, *3*, 1821−1826.
(43) Sun, H.; Cao, L.; Lu, L. *Nano Res.* **2011**, *4*, 550−562.

(44) Fan, Z.; Kai, W.; Yang, J.; Wei, T.; Zhi, L.; Feng, J.; Ren, Y.; Song, L.; Wei, F. *ACS Nano* **2011**, *5*, 191−198.
(45) Hummers, W. S.; Offeman, R. E. *J. Am. Chem. Soc.* **1958**, *80*, 1339.
(46) Liu, F.; Seo, T. S. *Adv. Funct. Mater.* **2010**, *20*, 1930−1936.